REVIEW

Check for updates

Challenges and advancement in direct ammonia solid oxide fuel cells: a review

Dattatray S. Dhawale, [iD] * Saheli Biswas, Gurpreet Kaur and Sarbjit Giddey [iD]

Finding solutions to tackle climate change and decarbonizing the energy sector are emerging as significant challenges for the global community. Carbon dioxide (CO_2) emission is the primary driver of global climate change, and therefore the world needs to urgently reduce CO_2 emissions by producing clean energy. Among the family of fuel cells, a solid oxide fuel cell (SOFC) is a high-efficiency power generation device with zero emission if hydrogen produced from renewable energy sources is used as a fuel. However, the utilization of hydrogen is restricted by the challenges related to its compression, storage, and transportation. Green ammonia contains 17.6 wt% hydrogen and is considered a suitable medium for hydrogen storage/carriage, facilitating CO_2-free energy systems, and so can play a critical role in the transition to clean energy. Therefore, green ammonia is an ideal carbon-free fuel for power generation in direct ammonia SOFCs (DASOFCs). In DASOFCs, ammonia cracks into hydrogen and nitrogen *in situ* in the anode chamber, and hydrogen is consumed in the electrochemical process; hence, there is no need for a separate ammonia cracking and hydrogen/nitrogen separation unit. Key technological challenges, though, must be addressed to realize the potential of green ammonia as a fuel in SOFCs. Therefore, the current review focuses on the role of ammonia as an energy carrier for power generation and discusses technological challenges such as ammonia safety, open circuit voltage (OCV) stabilization, thermal shocks, NO_x/N_2O emission, nitride formation, and nickel coarsening, limited power densities, and sealing issues, and the recent advancements in DASOFC technology. This review will also cover the performance of state-of-the-art anode materials and newly emerging proton-conducting materials for DASOFCs, along with the various approaches being used for the high-efficiency and long-term stability of DASOFCs in kilowatt (kW) scale systems. Finally, we address remaining challenges, discuss new opportunities, and suggest future recommendations for developing efficient DASOFC systems for the single-step conversion of ammonia to electricity.

1 Introduction

1.1 Global energy scenario

Worldwide energy and climate crises are the biggest concerns and have spurred interest in developing carbon-free energy. Tackling climate change issues and decarbonization is crucial to avoid impacting health, ability to grow food, safety, and work.[1] The global energy demand is growing from 16 terawatt (TW) in 2010 to 23 TW in 2030 and 30 TW in 2050, highlighting the importance of clean and sustainable energy sources.[2,3] Following the recent 2021 United Nations Climate Change Conference, more commonly referred to as COP26, held at the SEC center in Glasgow, United Kingdom, various countries committed to net-zero targets and have pledged their Nationally Determined Contributions to ensure the energy

transition and reduce emissions.[4] Fig. 1 represents the impact on emissions of replacing fossil fuels with renewables and increasing energy efficiency through to 2030.[5] As per the International Renewable Energy Agency (IRENA) 1.5 °C scenario, the emission reduction trajectory requires the deployment of technological avenues and a significant acceleration in renewable energy efficiency, electrification, hydrogen and derivatives needed to meet challenging milestones by 2030.[5] For a net-zero emission target for limiting the temperature increase to below 2 °C, green hydrogen is a central component for the deep decarbonization of our energy system. However, there are significant challenges related to hydrogen storage and transport (a very low volumetric energy density of 8 MJ L^{-1}, more than four times lower that of liquid hydrocarbon energy density), and safety challenges such as a low energy barrier for combustion in air, a large liquid-to-vapor volume expansion (860 times under ambient conditions), a low normal boiling point, and the fact that hydrogen can leak through and cause embrittlement in many materials due to its

CSIRO Energy, Private Bag 10, Victoria, Clayton South 3169, Australia.
E-mail: dattatray.dhawale@csiro.au

6176 | *Inorg. Chem. Front.*, 2023, **10**, 6176–6192

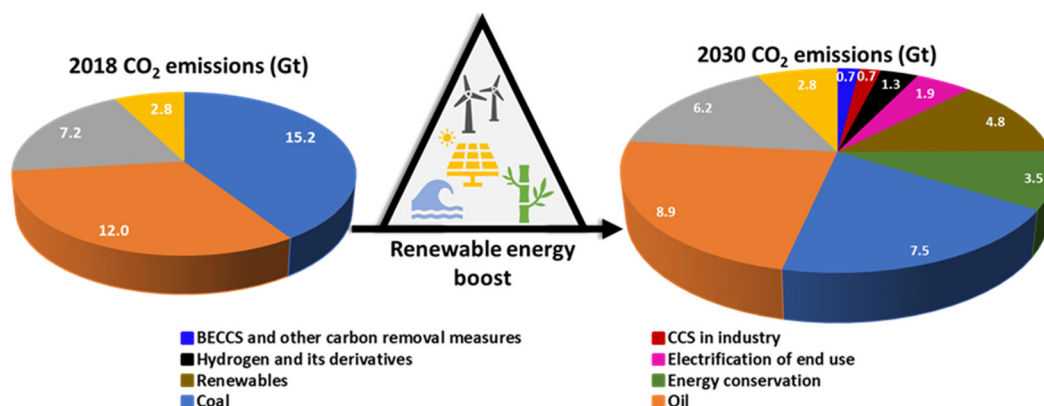This journal is © the Partner Organisations 2023

Fig. 1 The impact on emissions of replacing fossil fuels with renewables and increasing energy efficiency through to 2030. Note: Gt = gigatonne; CCS = carbon capture and storage; BECCS = bioenergy combined with carbon capture and storage.

molecular size. All these characteristics require special safety considerations and the need to build a new infrastructure for effective transportation or storage, which would further impact the logistical supply chain of hydrogen, limiting its use as a fuel in fuel cells for electric vehicles.[6] Chemical or physical bindings are potential alternatives to the supply chain that can support liquefication or compression. The chemical storage of hydrogen in the form of ammonia, methanol, and ethanol can alleviate hydrogen storage and safety issues.

1.2 Role of ammonia as an energy carrier

Among all chemicals, ammonia has the highest hydrogen content, can be stored as a liquid at moderate pressures and temperatures, and shipped over long distances due to the existing infrastructure, and then can be used as a source of hydrogen or in fuel cells and turbines for power generation without CO_2 emission. The specific energy of a tank filled with liquid ammonia is about two times higher than a tank filled with hydrogen at 700 bar.[7,8] Ammonia has had a profound global impact since the discovery of its synthesis from hydrogen and nitrogen by Haber and Bosch, now called the Haber–Bosch (H–B) process, which requires high temperature and pressure. With the established infrastructure, over the last decade, momentum has been shifted from the H–B ammonia industry using natural gas (NG) towards using renewable sources, as demonstrated by the opening of a pilot plant by Siemens in Oxfordshire, UK, in 2018 and Nel Hydrogen and Yara in Western Australia.[9] They have synthesized green ammonia from renewable electricity, water, and air, which could be a critical enabler of the global transition to sustainable energy and net-zero emission economies that can open significant markets and are positioned to play a vital role in the supply chain. So, there is unprecedented momentum worldwide to fulfill ammonia's longstanding potential as a clean energy solution. The high potential for liquid ammonia is not only due to its good hydrogen carrier capacity and versatility of application (fertilizer, fuel cells) but also because it contains almost three times as much energy as compressed gaseous hydrogen (700 bar), is equivalent to fossil fuels and emits

nearly zero emissions, as documented in the literature.[10,11] Another advantage of ammonia is the high maturity of its transportation and storage: worldwide >180 million metric tons of ammonia is produced annually; a vast ammonia infrastructure is already in place with 120 shipping ports equipped with ammonia terminals. In this regard, finding clean and reliable new energy conversion devices directly fueled by ammonia is of the utmost importance.

Green ammonia, as a fuel, offers many advantages, such as a high volumetric density of 5.2 kW h kg^{-1} (or 5.2 MW h per ton) and high hydrogen content of 5.88 kW h kg^{-1} (based on the LHV of H_2) of ammonia, theoretical hydrogen conversion efficiency of about 90%, ease of liquefaction and transport at ambient temperatures, and low cost.[12–14] Ammonia contains a higher hydrogen content (17.75 wt%) compared with methanol (12.6 wt%) and other chemicals. The ammonia has a high volumetric hydrogen density of 107.3 kg H_2 per m^3 compared with its liquid form or under pressure, as shown in Fig. 2,[15] which makes it attractive for energy storage and transport applications. Green ammonia synthesis using renewable resources and its applications are schematically presented in Fig. 3. Green ammonia has a significant impact by enabling
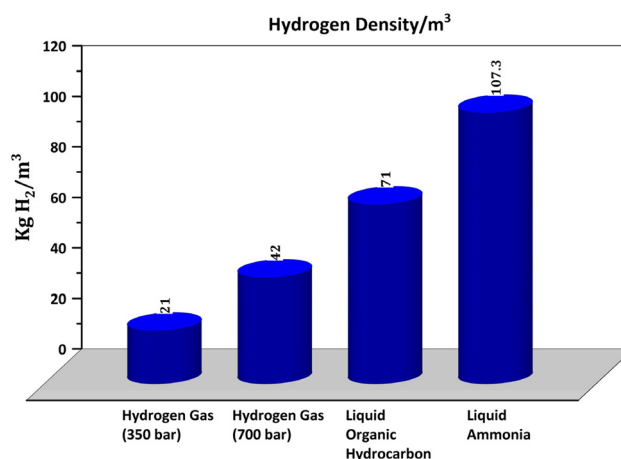

Fig. 2 Comparison of hydrogen storage density in different forms.

This journal is © the Partner Organisations 2023

Inorg. Chem. Front., 2023, **10**, 6176–6192 | **6177**

the transition from our global dependence on fossil fuels and contributing toward net-zero emissions from fertilizer and power generation sectors mainly using fossil fuels.[16,17] Green ammonia can be synthesized using hydrogen produced by electrolyzers operated by renewable sources and atmospheric nitrogen. Recently, Jupiter Ionics electrolysis technology demonstrated green ammonia production technology for small-scale applications.[18] Ju *et al.*[19] and MacFarlane *et al.*[20] synthesized green ammonia by the alkaline electrochemical reduction of nitrogen at ambient temperature and pressure.

Ammonia can be utilized as a fuel in different energy systems, and the oxidation reaction of ammonia is exothermic, which can produce heat; thus, all internal and external combustion technologies could be fueled by ammonia.[21] However, the emission of NO_x cannot be avoided due to a high combustion temperature, and even NO_x emission increases due to the presence of nitrogen in the fuel. Another approach to using ammonia as a fuel in energy systems is to decompose ammonia into hydrogen and nitrogen and then use hydrogen as a well-known fuel in fuel cells and combustion systems.[22]

Therefore, an innovative approach is the use of green ammonia as a direct fuel in high-temperature SOFC systems. This is a more attractive option for "single-step ammonia to electricity" generation because of its capability of *in situ* ammonia cracking/decomposition and fuel cell operation (power generation), which can offer high efficiencies for future combined heat and electricity production and transportation.[23] As ammonia cracking/decomposition is an endothermic reaction, $\Delta H = +45$ kJ per mole, the high-temperature operation of SOFC and the heat generated within the SOFC cells (due to resistive losses) can assist this process. Also, the

zirconia-based solid electrolyte is stable, and SOFCs have better compatibility with ammonia fuel. Therefore, direct ammonia-fuelled SOFC (DASOFC) has the potential and can provide a pathway to decarbonize various applications reliant on fossil fuels.[23–25]

1.3 Fundamental operating principles of ammonia SOFCs

Among the family of fuel cells, because of the high-temperature operation, a solid oxide fuel cell (SOFC) is the most efficient electrochemical energy conversion device, which directly converts chemical energy to electricity by oxidizing fuels. Typically, it consists of a dense, non-porous oxygen ion-conducting or proton-conducting solid electrolyte (usually a ceramic) membrane positioned between a cathode and an anode, and it operates at high (600–1000 °C) temperatures. This enables favorable kinetics that allows the use of relatively cheap nickel or cermet (composite) electrodes, and the thermal heat produced in the process can contribute towards achieving a high combined heat and power (CHP) efficiency. With green ammonia as a fuel for SOFCs, there is no need for an external ammonia cracker or separation unit, which can offer several advantages over hydrogen fuel. The principle of a direct ammonia solid oxide fuel cell based on oxide-ion-conducting (O-DASOFC) and proton-conducting (H-DASOFC) electrolytes is presented in Fig. 4.

In the DASOFC system, ammonia is cracked at elevated temperatures, ranging between 500 and 1000 °C. An advantage of using such high temperatures is that the cracking of ammonia and the electricity generation process can effectively be merged. Ammonia can therefore be directly fed into SOFCs, eliminating any pre-treatment requirement. The potential use of ammonia for alkaline fuel cells was first investigated by

Fig. 3 The landscape of green ammonia synthesis and its use in different sectors.

Fig. 4 Schematic representation of a direct ammonia solid oxide fuel cell based on oxide-ion-conducting (O-DASOFC) and proton-conducting (H-DASOFC) electrolytes.
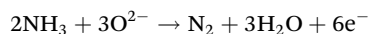
Cairns et al.[26] Later, in the 1980s, Vayenas and Farr et al.[27] demonstrated the use of ammonia as a fuel for SOFCs using platinum electrodes for electricity and nitric oxide generation. Since then, many researchers have considered ammonia a direct fuel for SOFC. This DASOFC technology delivers the highest round-trip electric (50–55%) and thermal (30–40%) efficiencies for ammonia utilization.[13] In general, the reaction mechanism of SOFC fueled by ammonia fuels proceeds in two ways. In the first case, endothermic ammonia cracking can occur inside the fuel cell stack over the Ni-YSZ anode, with hydrogen being used in the exothermic electrochemical reaction, which benefits from high thermodynamic efficiency.

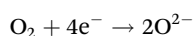The overall reaction for direct ammonia-fueled SOFCs is as follows,

$$2NH_3 + 1.5O_2 \rightarrow N_2 + 3H_2O \text{ (in situ and in-operando cracking)}$$
(Ammonia FC reaction)
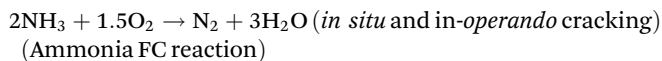
The supplied oxygen at the cathode (e.g., LSCF) is reduced to O^{2-} ions that are transported through the dense electrolyte O-SOFC (typically yttria-stabilized zirconia) and react with hydrogen generated from ammonia over the anode catalyst (Ni-YSZ) to form H_2O.
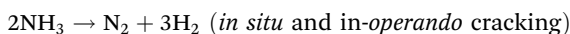
The possible anodic reactions for ammonia are as follows,

$$2NH_3 + 3O^{2-} \rightarrow N_2 + 3H_2O + 6e^-$$

$$2NH_3 + 5O^{2-} \rightarrow 2NO + 3H_2O + 10e^-$$

$$2NH_3 + 3NO \rightarrow \frac{5}{2}N_2 + 3H_2O$$

And the corresponding cathodic reaction is

$$O_2 + 4e^- \rightarrow 2O^{2-}$$

In the second case, ammonia decomposes into nitrogen and hydrogen as per the below equation

$$2NH_3 \rightarrow N_2 + 3H_2 \text{ (in situ and in-operando cracking)}$$

and then the power generation takes place as per the following reaction.

$$H_2 + O^{2-} \rightarrow H_2O + 2e^- \text{ (hydrogen FC reaction)}$$

The feasibility of the direct utilization of ammonia as a fuel in SOFCs has been well documented in the literature and patents,[28–35] and some excellent reviews have discussed the progress of ammonia-fed SOFC technology.[12,13,23–25,27,36–44] Therefore, DASOFC becomes a key element of a net-zero energy mix for power generation. However, due to the use of ceramic solid electrolytes in SOFCs, the operating temperature is as high as 600–850 °C or above. Due to such high operation temperatures, there is a strong possibility of ammonia decomposition into N_2 and H_2. Other technological challenges, such as microstructural changes, nitride formation, NO_x formation, and efficiency and performance durability at the larger scale, remain for direct ammonia solid oxide fuel cells.

Therefore, this review discusses the fundamental issues and technological challenges associated with DASOFCs, their operating principle, and the performance of state-of-the-art and newly emerging materials for DASOFCs. Then, the concept of DASOFCs will be validated and demonstrated by versioned approaches toward scale-up (kW) and long-term stability. Finally, we discuss the challenges and opportunities and offer future recommendations in the DASOFC field.

2 Technological challenges in DASOFCs

Although using ammonia as a fuel in SOFC systems has substantial benefits, it is associated with a few technological challenges and drawbacks, such as the safety of the ammonia, OCV stabilization, thermal shocks, NO_x/N_2O emission, nitride formation, and nickel coarsening, limited power density and sealing issues—the details of each are outlined below.

2.1 Ammonia safety

As high-energy density carriers like ammonia are very reactive, the risk of explosion is an essential safety concern in its transportation. Ammonia has a narrow range that limits its flammability in the air. Great care is required to prevent and control the leakage of ammonia gas because of its toxicity, and pro-

This journal is © the Partner Organisations 2023

Inorg. Chem. Front., 2023, **10**, 6176–6192 | **6179**

longed exposure to a high concentration of ammonia can have severe health effects or even cause death.[45] It has been demonstrated that these risks can be effectivity mitigated using well-established industry best practices.[46] Comparing the toxicity with gasoline and methanol, liquid ammonia is three orders of magnitude higher in "apparent toxicity", *i.e.*, the vapor pressure relative to the toxicity at room temperature.[47] However, ammonia has a distinct pungent smell and can be detected by the human nose at a concentration as low as 20 ppm in air, allowing preventative measures to be immediately in place.[11] Because of its toxicity, ammonia can be stored in metal salts and released reversibly at around 250 °C.[48] Another disadvantage of using ammonia as a hydrogen carrier is that trace amounts of ammonia can be found in the hydrogen even after decomposition,[48] implying lower ammonia conversion and poisoning the cells, especially in PEMFCs. Notably, unlike gasoline, which contains carcinogenic substances such as benzene, ammonia is not considered carcinogenic.

2.2 OCV stabilization

A high open circuit voltage (OCV) is important in electrochemical systems to achieve high fuel conversion efficiencies. The theoretical open circuit voltage for a hydrogen solid oxide fuel cell at 800 °C should be around 1 V, and for ammonia fuel cells, it should be >1.2 V.[49] Usually, the reversible cell voltage decreases with temperature for hydrogen oxidation reactions whereas it increases for ammonia oxidation due to changes in entropy and Gibbs free energy. However, few studies have shown different open circuit voltages for ammonia-fed solid oxide fuel cells.[40] This could be due to multiple factors. (1) Catalytic thermal decomposition of ammonia in particular conditions could significantly impact the OCV due to variations in partial pressure of the hydrogen. For example, Fuerte *et al.*[50] observed a decreased OCV in mixed humidified conditions for hydrogen and ammonia-fed fuel cells. This has also been explained in detail by a review of the decomposition of ammonia to produce hydrogen reported by Lucentini *et al.*[51] (2) OCV variation could also be due to the presence of microcracks, especially in thin electrolytes. Furthermore, multiple articles reported low OCV due to electrolyte properties, such as mixed ionic and electronic conductivity in doped ceria.[52] However, further research must be conducted to elucidate reaction mechanisms using standard state-of-the-art systems.

2.3 Thermal shocks

Thermal shocks during intentional or emergency shutdowns can degrade the performance of ammonia-fed solid oxide fuel cells. In such cases, a similar thermal expansion coefficient of SOFC materials is very important to avoid an interruption in the ionic and electronic pathways and a delamination of the interfaces.[53] The thermal expansion coefficients of some of the SOFC materials, interconnects, and sealants lie in the range of $10.5–13.9 \times 10^{-6} \ K^{-1}$.[54] For example, to provide thermal compatibility between electrodes and electrolytes, composites such as cathodes made with $Sm_{0.5}Sr_{0.5}CoO_{3-\delta}$ (SSC) and ceria-based

electrolytes have shown better thermal resistance than $Sm_{0.5}Sr_{0.5}CoO_{3-\delta}$ (SSC) to match compatibility with ceria electrolytes.[55] In addition, in ammonia-fueled solid oxide fuel cells, with state-of-the-art nickel-based electrodes, nitridation of the electrodes during thermal cycling occurs, which could result in severe performance degradation due to irreversible morphological changes in the anode microstructure and respective electrochemical properties.[36,56] The extent of nitrification depends upon the ammonia cracking reaction rate.[57] Other non-metallic electrodes could be the possible solution to minimize the impacts of thermal cycling and nitrification. During cell operation, thermal shocks could also occur due to a decrease in the cell temperature caused by the endothermic ammonia decomposition reaction. Kishimoto *et al.*[58] have tested SOFC stacks consisting of 30 planar anode-supported cells with an active area each of 95 cm². They observed a slight temperature drop of 15 K. However, it might be a concern with larger stacks and needs to be investigated thoroughly. Especially with high flow rates and concentrated ammonia, a significant drop in cell performance has been observed by Miyazaki *et al.*[59]

2.4 NO$_x$/N$_2$O emission

The emission of toxic NO$_x$/N$_2$O can impact air quality, leading to human and environmental concerns. In SOFCs based on an oxygen-ion conducting electrolyte such as YSZ, oxygen ions are transported from the cathode to the anode and react with ammonia or nitrogen produced by ammonia cracking in the anode chamber, and there is a possibility of NO$_x$/N$_2$O emission[60] as per the below equation.

$$2NH_3 + 5O^{2-} \rightarrow 2NO + 3H_2O + 10e^-$$

If the H$_2$O is generated at the fuel electrode side, the exhaust gas would contain a mixture of steam and a small amount of unconverted ammonia, which, when cooled in the exhaust, yields a very corrosive liquid or NO$_x$ when combusted. To avoid the emission of toxic NO$_x$/N$_2$O and improve the DASOFC performance, the use of proton-conducting electrolytes such as doped BaCeO$_3$ is highly recommended.[61] When the proton transfers from the anode to the cathode through the proton-conducting electrolyte, H$_2$O is produced in the cathode chamber, eventually minimizing the corrosion issues and reducing the generation of NO$_x$ from electrochemical oxidation.[24] It is also noted during DASOFC, and unused ammonia in anode off-gas could be easily removed by a high-temperature catalytic reaction.

2.5 Nitride formation and nickel coarsening

When ammonia is fed to the SOFC system for power generation and if the ammonia is not fully cracked, there is a strong possibility that the nickel surface of the anode (Ni-YSZ) might convert into nitride (Ni$_3$N), resulting in volumetric changes in the anode microstructure of the cell, an increase in ohmic overpotential, and electrode delamination. Additionally, materials widely used in the Ni-YSZ anode must resist redox

6180 | *Inorg. Chem. Front.*, 2023, **10**, 6176–6192

This journal is © the Partner Organisations 2023

reactions to crack the ammonia fuel; otherwise, nickel particles in the Ni-YSZ anode can form Ni_3N. This redox reaction can cause cell degradation or even electrolyte cracking by increasing the interfacial polarization between the electrolyte and anode. Stoeckl and Kishimoto[56,58] reported SOFC stack performance degradation under ammonia fuel due to the nickel catalyst causing nitride formation. They also observed that the temperature drop had affected the stack performance due to the ammonia's endothermic reaction, leading to a lower decomposition rate. Yang et al.[36] found that Ni nitride formation results in morphological and structural changes in the Ni-YSZ anode, which affects the long-term stability of DASOFC with the Ni-YSZ anode. Fig. 5(a) shows the XRD pattern of the state-of-the-art Ni-YSZ anode material for an SOFC under ammonia fuel and how Ni turns into Ni_3N during the long-term test. Also, nickel coarsening and thermal stresses may lead to accelerated degradation.

These results conclude that nickel particles in the Ni-YSZ cermet anode can turn into Ni_3N under a pure ammonia atmosphere as per the following reaction;

$$3Ni + NH_3 \rightarrow Ni_3N + 1.5H_2$$

Stoeckl et al.[56] reported on investigations of anode microstructural changes of the cell, suggesting nickel nitriding formation. As shown in Fig. 5(b), they also observed Ni particle enlargement, the appearance of microscopic pores, and agglomerations in the metallic nickel particles due to their nitridation.

2.6 Limited power densities

At the stack and system level cells, the limited power density is one of the technological concerns in DASOFCs. One way to achieve higher power densities at a larger scale is by further reduction of the electrolyte thickness by depositing the same as a nanostructured thin layer using a technique known as pulsed laser deposition (PLD)[62–64] (Fig. 6(a)). This new fabrication technique has led to the emergence of what are known as thin-film SOFCs. Recently, Oh et al.[62] tested thin-film DASOFC with a Ni-GDC anode, 8YSZ electrolyte and LSCF-GDC cathode at 650 °C, achieving a peak power density of 1330 mW cm^{-2}, which is the best performance reported to date. The authors proposed that incorporating a more active ammonia decomposition catalyst will improve the performance of low-temperature thin-film DASOFCs. The same concept can also be extended to electrodes, whereby the electrodes are fabricated using PLD. For example, Myung et al.[63] tested a pulsed laser-deposited LSC-GDC composite (LSC-GDC$_{PLD}$) cathode for H$_2$-SOFC and obtained a peak power density of 850 mW cm^{-2} at 650 °C, which was initially slightly lower than a conventional single layer LSC-GDC cathode (LSC-GDC$_{SLD}$). However, after 12 h of continuous operation at 0.7 V, the polarization resistance of the LSC-GDC$_{PLD}$ remained almost unchanged, whereas that of the LSC-GDC$_{SLD}$ increased nearly ten times. The observation is quite promising and worthy of investigation for DASOFCs. Another emerging fabrication technique is atomic layer deposition[65] (Fig. 6(b)), where the ceramic and/or metal precursors assisted by organic or organometallic ligands are deposited as self-assembled functional layers on a substrate, one on top of the other. This gives a highly precise and controlled nanostructured surface that has been shown to not only improve the reaction kinetics but also alleviate issues related to microstructural delamination.[66–69] However, this technique has so far not been employed for DASOFCs and is definitely worthy of further investigations.

2.7 Sealing issues

Sealing is required for manifolds holding ceramic cells to avoid fuel crossover. Thermal stresses due to thermal shocks can fracture seals which is a big concern in high-temperature cell operations. Therefore, seals should have mechanical
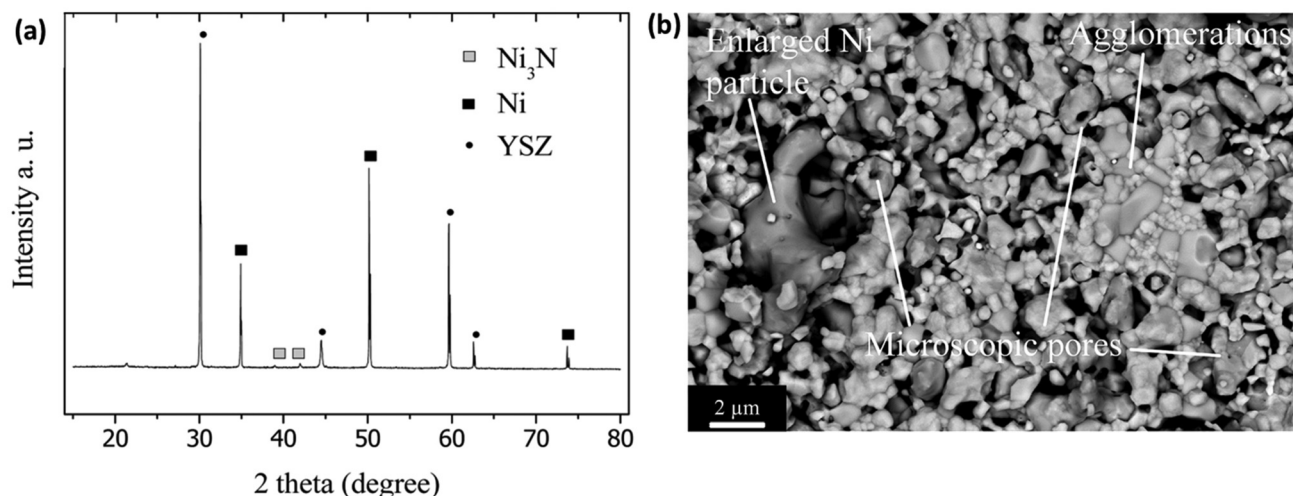

Fig. 5 (a) XRD pattern of Ni film on a YSZ disk after exposure to ammonia (100 mL min^{-1}) at 600 °C for 1 h. Reproduced with permission.[36] Copyright 2015, American Chemical Society. (b) SEM image of the anode surface at the fuel inlet region. Reproduced with permission.[56] Copyright 2019, Elsevier.

This journal is © the Partner Organisations 2023

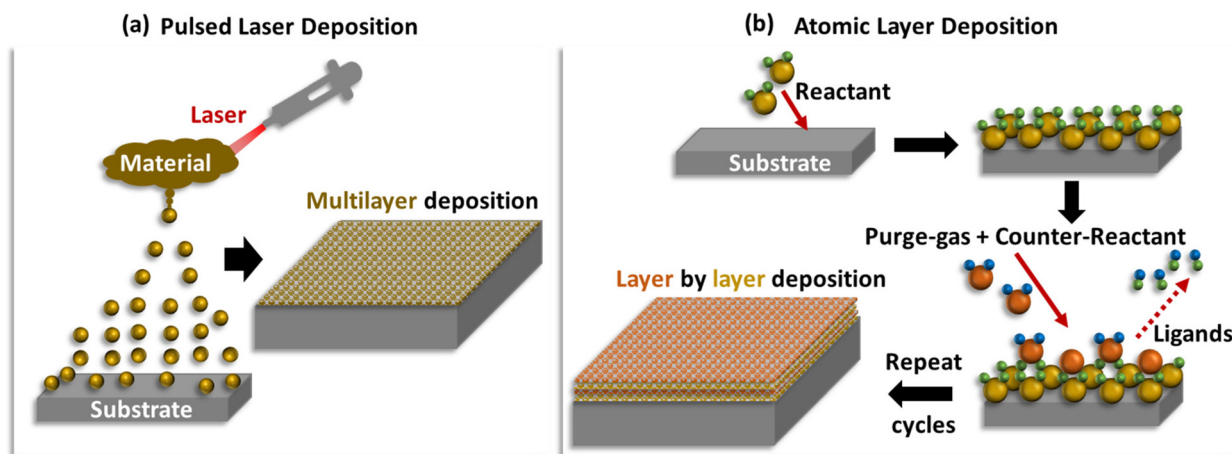Inorg. Chem. Front., 2023, **10**, 6176–6192 | **6181**

Fig. 6 Schematic representations of (a) pulsed laser deposition and (b) atomic layer deposition techniques.

strength and be made of compatible thermal materials like ceramic cells. In addition, sealing materials should not be electrically conducting, which could cause the shortening of the cells.

Importantly, sealing materials should be chemically stable in different fuel environments and resistant to hydrogen embrittlement. Detailed information on different types of seal, such as rigidly bonded seals, compressive seals, and compliant bonded seals, is well-reported in the literature.[70] However, there is not much information available in the literature on the compatibility of existing sealants under an ammonia atmosphere. Diluted ammonia can be the safest option with existing systems for ammonia fuel cells, as per existing studies conducted using direct ammonia SOFCs. In such a regard, a tubular design instead of a planar design can simplify the sealing challenges as no sealing is required inside the hot zone.

3 State-of-the-art and newly emerging anode materials for DASOFCs

The first DASOFC comprising a dense 8YSZ electrolyte was tested back in the 1980s by Vayenas *et al.*[71] Following this, Wojcik *et al.*[72] tested an 8YSZ electrolyte supported planar DASOFC with silver/platinum electrodes and an iron catalyst, and obtained a maximum power density of 50 mW cm^{-2} at 800 °C. These two pioneering works led to growing interest in DASOFC, and a substantial advancement in electrocatalytically active electrode materials has been made ever since. The 8 mol% yttria-stabilized zirconia (8YSZ) is the most mature and conventional electrolyte for SOEC/SOFC systems due to its excellent mechanical strength and stability, and appreciable ionic conductivity at higher temperatures (800 to 1000 °C). Other promising electrolytes are scandia-doped ceria ($Ce_{0.8}Sm_{0.2}O_{2-\delta}$, SDC)[73,74] and lanthanum strontium magnesium gallate (LSGM);[75,76] however, these are limited by their

power densities. Lanthanum-based perovskites like $La_xSr_{1-x}Co_yFe_{1-y}O_3$ (LSCF), $La_xSr_{1-x}CoO_3$ (LSC) and $La_xSr_{1-x}MnO_3$ (LSM) have been unanimously agreed upon as the most suitable cathode materials for their high mixed ionic electronic conductivity. However, cobalt or cobalt–iron as the B-site cation has usually shown a better performance than manganese due to a lower Co–O bond strength than Mn–O, which allows easy lattice-hopping of oxide ions and oxygen vacancy formation.[77] In recent times, other perovskites, double perovskites, spinel oxides, and Ruddlesden–Popper (RP) structures have also shown promise as cathode materials. Zhong *et al.*[78] tested cobalt-based spinel ACo_2O_4 (A = Zn, Fe, Ni) oxides with different A-site cations as DASOFC cathodes, and their structural analysis based on XRD, XPS, and UV-Vis diffuse reflectance revealed that $NiCo_2O_4$ exhibited higher electronic conductivity and better adhesion with the electrolyte. Furthermore, the surface was rich in Co^{3+}, leading to better oxygen vacancy formation. The maximum power densities at 800 °C followed the order $NiCo_2O_4$ (1060 mW cm^{-2}) > $FeCo_2O_4$ (920 mW cm^{-2}) > $ZnCo_2O_4$ (830 mW cm^{-2}). Further details on SOFC cathodes have been extensively discussed in other reviews.[25,79]

Most of the research on DASOFCs has focused on anode development since the overall rate-determining electrocatalytic reactions occur at the anode. As shown in Fig. 7, the ideal anode for a high-performing DASOF should have (1) excellent catalytic activity towards NH_3 decomposition to guarantee complete decomposition before it reaches the triple phase boundary (TPB) in order to avoid undesired side reactions of unconverted NH_3 with oxide ions; (2) sufficient porosity to ensure an easy bulk diffusion of gases (NH_3, H_2, N_2, steam); (3) appreciable ionic as well as electronic conductivity that would enlarge the TPB and improve overall cell kinetics; and (4) thermal expansion coefficient compatibility with the electrolyte to ensure proper adhesion. In view of these four criteria, Ni-based ceramic-metallic (cermet) materials have gained a lot of attention, the most widely studied one being Ni-YSZ due to

6182 | *Inorg. Chem. Front.*, 2023, **10**, 6176–6192

This journal is © the Partner Organisations 2023

Properties of ideal DASOFC anode

Fig. 7 The schematic shows the four essential properties of the ideal anode material for DASOFC.

its good catalytic activity towards the NH_3 decomposition reaction.[80]

3.1 Cermet anodes

Cinti et al.[32] have demonstrated a thermodynamic model using anode-supported Ni-8YSZ cermet (~1500 μm) for a complete SOFC stack operation for ammonia fuel. The results show that ammonia-fuelled SOFC is more efficient than hydrogen-fuelled due to the cooling effect of internal reactions that reduces the ancillaries' energy consumption related to cathode airflow. Ma et al.[81] tested an anode-supported cell with an 8YSZ electrolyte, NiO-YSZ anode, and LSC-GDC cathode and obtained a maximum power density of 526 mW cm^{-2} at 850 °C, which was comparable to that obtained with H_2 as the fuel. Yang et al.[36] tested a Ni-YSZ anode-supported planar cell with a 8YSZ electrolyte and a composite of gadolinia-doped ceria ($Ce_{0.8}Gd_{0.1}O_{2-\delta}$, GDC) and lanthanum strontium cobalt ferrite ($La_{0.6}Sr_{0.4}Co_{0.2}Fe_{0.8}O_{3-\delta}$, LSCF) cathode, reporting a maximum power density of 325 mW cm^{-2} at 700 °C. Recently, Shy et al.[82] tested the performance of an anode-supported cell with a Ni-YSZ anode, a 8YSZ electrolyte, and a composite of GDC and LSC cathode between 750 and 850 °C and at pressures of 1 atm and 3 atm. The power density increased as a function of temperature and pressure. For instance, at 800 °C, the power density increased from 1100 mW cm^{-2} at 1 atm to 1350 mW cm^{-2} at 3 atm, as shown in Fig. 8(a). The electrochemical impedance spectral analysis revealed that increasing the pressure reduced the gas diffusion resistance while slightly increasing the gas conversion resistance. The positive effect of pressurization has been reported in another study,[83] where the power densities obtained at 0.7 V at 1/3/5 atm pressures were

160/228/266 mW cm^{-2} at 750 °C, 274/377/414 mW cm^{-2} at 800 °C and 389/451/506 mW cm^{-2} at 850 °C (Fig. 8(b)).

Ceria-based materials with excellent mixed ionic electronic conductivity and phase compatibility with YSZ have also attracted many researchers. A Ni-SDC anode-supported DASOFC with a 10 μm thick SDC electrolyte and a $Ba_{0.5}Sr_{0.5}Co_{0.8}Fe_{0.2}O_{3-\delta}$ (BSCF) cathode yielded a maximum power density of 1190 mW cm^{-2} at 650 °C (Fig. 8(c)), which was considerably lower than that obtained with H_2 as the fuel (1872 mW cm^{-2}).[33] This performance gap was attributed to the actual temperature drop inside the cell brought about by the endothermic nature of the ammonia decomposition reaction. Ma et al.[74] tested a DASOFC comprising a 50 μm thick SDC electrolyte sandwiched between a Ni-SDC anode and $Sm_{0.5}Sr_{0.5}CoO_{3-\delta}$ (SSC)-SDC cathode and reported maximum power densities of 168.1 and 191.8 mW cm^{-2} at 600 °C with NH_3 and H_2 as the fuels, respectively.

The cell exhibited no performance degradation over 50 h at 0.45 V, producing a stable current density of 360 mA cm^{-2} (power density 162 mW cm^{-2}). However, Ni as the catalyst metal poses several challenges, as mentioned in the previous section. This has led to substantial interest in studying other monometallic as well as bimetallic cermet compositions. Akimoto et al.[76] systematically evaluated the performance of SDC-based cermet with Ni, Co, Fe, and 40%Ni–60%Fe as the metal phase in a planar LSGM electrolyte-supported cell with a Pt cathode. Maximum current densities at 900 °C followed the order Ni–Fe (360 mA cm^{-2}) > Fe (242 mA cm^{-2}) > Ni (120 mA cm^{-2}) > Co (85 mA cm^{-2}). However, the high sinterability of Fe calls for testing the short-term as well as long-term stability of Fe and Ni–Fe alloy-based cermets. In another study,[75] 97%Ni–

This journal is © the Partner Organisations 2023

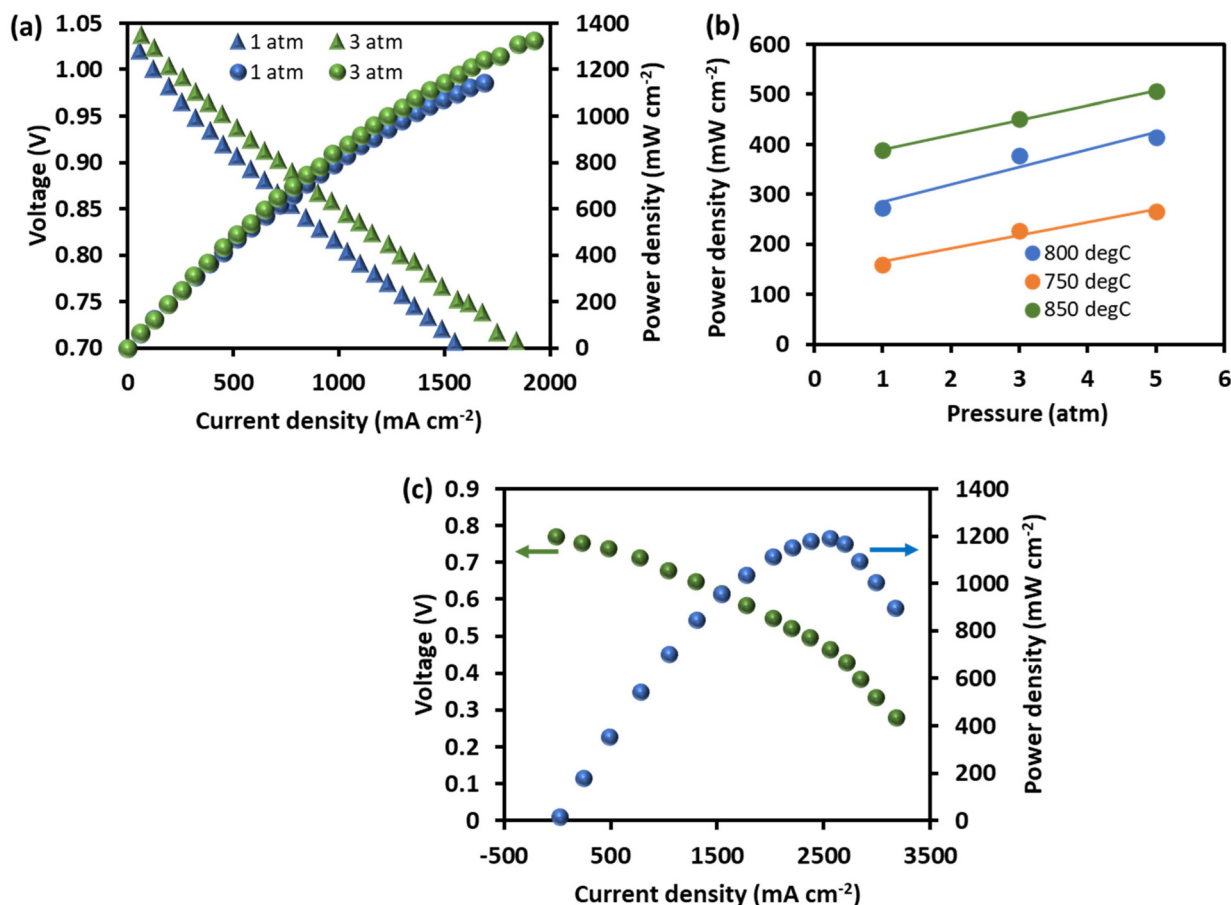Inorg. Chem. Front., 2023, **10**, 6176–6192 | **6183**

Fig. 8 Power density and voltage as a function of current density for (a) anode-supported DASOFC with a Ni-YSZ anode, an 8YSZ electrolyte, and a composite cathode of GDC and LSC at 800 °C under pressures of 1 atm and 3 atm,[82] Copyright 2018, Elsevier, (b) power density as a function of temperature and pressure and (c) a Ni-SDC anode-supported DASOFC with a 10 μm thick SDC electrolyte and a $Ba_{0.5}Sr_{0.5}Co_{0.8}Fe_{0.2}O_{3-\delta}$ (BSCF) cathode.[33] Copyright 2007, Elsevier. All plots were redrawn from the original papers.

3%M* (M* = Mo, W, Ta) alloy-based SDC anodes were studied at 900 °C to understand the effect of the promoter M*. Maximum power densities followed the order Mo (416 mW cm^{-2}) > Ta (322 mW cm^{-2}) > W (313 mW cm^{-2}) > Co (85 mW cm^{-2}). While Mo accelerated NH_3 adsorption and nitride formation, pristine Ni enhanced N_2 desorption, and according to the authors, a synergy of these two effects improved the overall cell kinetics for NH_3 oxidation. Nonetheless, the long-term stability of all such Ni-based materials needs to be investigated before their superior performance as DASOFC anodes can be vouched for.

3.2 Perovskite anodes

Over the past few years, perovskites, double perovskites, spinel oxides, and pyrochlore oxides have also been widely studied as prospective DASOFC anode materials. Rathore et al.[84] evaluated a Pd nanoparticle-infiltrated Ag-LSCF composite anode at 800 °C and reported a 43% performance improvement compared with bare Ag-LSCF. The authors concluded that Pd nanoparticles in the anode provided hydrogen dissolution that shifted the ammonia decomposition reaction forward, thus

improving the overall cell kinetics. Our group also recently reported the feasibility of a DASOFC for power generation employing a 3YSZ electrolyte-supported Pd–Ag-LSCF symmetric cell and achieved a power density of 73 mW cm^{-2} at 800 °C with ammonia fuel.[23] The low power density is due to poor electrolyte-supported cell structure, such as the thick 3YSZ electrolyte (~300 μm), and the lower catalysis activity of the electrode materials. Recently, Cavazzani et al.[85] studied a composite of 8YSZ and Ni-doped $La_{0.45}Sr_{0.45}TiO_3$ synthesized via sol–gel technique as a DASOFC anode at 780 °C in 40% $NH_3/60\%Ar$ and achieved a peak power density of 3.7 mW cm^{-2}.

Song et al.[73] tested an SDC-supported cell with a $La_{0.52}Sr_{0.28}Ti_{0.94}Ni_{0.03}Co_{0.03}O_{3-\delta}$ (LSTNC) anode and $Ba_{0.5}Sr_{0.5}Co_{0.8}Fe_{0.2}O_{3-\delta}$ (BSCF) cathode and achieved a power density of 361 mW cm^{-2} at 800 °C. Interestingly, the cell was stable over a continuous operation of 120 h, which was attributed to the exsolution of strongly coupled Ni–Co nanoparticles. In another recent study, Ru-doped $Pr_{0.6}Sr_{0.4}Co_{0.2}Fe_{0.75}Ru_{0.05}O_{3-\delta}$ single-phase perovskite gave a maximum power density of 500 mW cm^{-2} with 100% NH_3 conversion at 800 °C.[86] In a reducing atmosphere, $Pr_{0.6}Sr_{0.4}Co_{0.2}Fe_{0.75}Ru_{0.05}O_{3-\delta}$ decom-

6184 | Inorg. Chem. Front., 2023, 10, 6176–6192

This journal is © the Partner Organisations 2023

posed to Pr_2O_3 nanoparticles and $Pr_{0.6}Sr_{0.4}Co_{0.2}Fe_{0.8}O_{3-\delta}$, accompanied by the exsolution of CoFeRu-based alloy nanoparticles that improved the catalytic activity, anti-sintering capability, and stability of the anode. Zhong et al.[87] studied pyrochlore $Pr_2B_2O_7$ oxides (B = Zr, ZrSn, Sn) and perovskites (B = Ti) as cathodes with 8YSZ electrolyte. It was found that $Pr_2Zr_2O_7$ with B-site cationic defects depicted enhanced ionic and electronic transport with power densities peaking at 1220 mW cm^{-2} at 800 °C and 250 mW cm^{-2} at 600 °C. Next, the same experiments were repeated but with $Sr_{1+x}Y_{2-x}O_{4+\delta}$ (SYO)-YSZ as the cathode, resulting in power densities of 240 mW cm^{-2} and 1210 mW cm^{-2} at 600 and 800 °C, respectively.[88] Interestingly, no performance degradation was seen even after 100 h of continuous operation.

In the scope of thermocatalytic ammonia cracking, the most precious metals used as catalysts include chromium (Cr), cobalt (Co), copper (Cu), iron (Fe), iridium (Ir), nickel (Ni), palladium (Pd), platinum (Pt), rhodium (Rh) and ruthenium (Ru) on metal oxides.[89–92] The catalytic activity and performance of different metal catalysts follow the order of Ru > Ni > Rh > Co > Ir > Pt $\cong$ Fe > Cr > Pd > Se $\cong$ Cu > Te > Pb, respectively.[92] By far, Ru-based catalysts have shown the highest ammonia conversion, but the high cost associated with Ru calls for finding other alternative materials or implementing advanced techniques like 3D printing to achieve higher performance with metals like Fe or Ni.[93,94] It is to be noted that the catalytic activity also varies according to ammonia concentrations and different types of support material, such as Ni/Y_2O_3 > Ni/Gd_2O_3 > Ni/Sm_2O_3 > Ni/La_2O_3 > Ni/Al_2O_3 > Ni/CeO_2.[93] Thus, oxide supports can be tailored to increase the surface area of the catalyst and promote selective surface adsorption/desorption processes. However, there is dearth of research related to Ru-based anode compositions for DASOFCs in the literature.

3.3 Emerging materials for proton-conducting DASOFCs

As already mentioned, one of the significant issues with DASOFC is NO_x poisoning at the anode, which can be avoided entirely in proton-conducting direct ammonia fuel cells. Moreover, they do not suffer from fuel dilution at the anode[95] and improve ammonia cracking by reducing the hydrogen-poisoning effect on Ni.[59,96] As an electrolyte, $BaCeO_3$-based materials have been most widely studied, which includes $BaCe_{0.8}Y_{0.2}O_{3-\delta}$,[97] $BaCe_{0.2}Zr_{0.7}Y_{0.1}O_{3-\delta}$,[98] $Ba_{0.9}K_{0.1}Ce_{0.6}Zr_{0.2}Y_{0.2}O_{3-\delta}$,[99] and $Ba_{0.8}Sr_{0.2}Ce_{0.6}Zr_{0.2}Y_{0.2}O_{3-\delta}$.[100] However, their ionic conductivities (~0.01 S cm^{-1}) are much less than typical oxide ion-conducting electrolytes like 8YSZ (~0.05 S cm^{-1}) and ScSZ (~0.07 S cm^{-1}), which limits their power densities and cell performance. For example, Maffei et al.[101] tested $BaCe_{0.8}Gd_{0.15}Pr_{0.05}O_{3-\delta}$ (BCGP) as an electrolyte, $NiO-BaCe_{0.85}Eu_{0.15}O_3$ (BCE) as an anode, and Pt as a cathode, and the peak power density at 600 °C was as low as 28 mW cm^{-2}. Pelletier et al.[102] used $BaCe_{0.8}Gd_{0.19}Pr_{0.01}O_{3-\delta}$ (BCGP) as an electrolyte, achieving a peak power density of 35 mW cm^{-2} at 700 °C. Zhang et al.[103] evaluated $BaCe_{0.8}Gd_{0.2}O_{3-\delta}$ (BCGO) as an electrolyte, $Ni-Ce_{0.8}Gd_{0.2}O_{1.9}$ (CGO) as an anode, and $Ba_{0.5}Sr_{0.5}Co_{0.8}Fe_{0.2}O_{3-\delta}$ (BSCFO)–CGO as a cathode and obtained a maximum power

density of 147 mW cm^{-2} at 600 °C due to the complete decomposition of NH_3. Lin et al.[104] tested $BaZr_{0.1}Ce_{0.7}Y_{0.2}O_{3-\delta}$ (BZCY) electrolyte with a NiO-BZCY anode and $Ba_{0.5}Sr_{0.5}Co_{0.8}Fe_{0.2}O_{3-\delta}$ (BSCF) cathode and obtained a maximum power density of 390 mW cm^{-2} at 750 °C. However, using the same BZCY electrolyte, Aoki et al.[105] reported a power density of 580 mW cm^{-2} at 600 °C using a Pd anode and LSCF cathode. According to the authors, the high H_2 splitting catalytic activity of Pd allowed the incorporation of a large number of protons in the Pd-BCZY interfacial region, accelerating the anodic charge transfer reaction. Some researchers have shown that the incorporation of a catalyst layer improves the performance of proton-conducting direct ammonia fuel cells by enhancing the anode's electrocatalytic activity and charge transfer at the anode–electrolyte interface. In this regard, Pd[106] and Fe[107] catalysts have shown peak power densities of 724 mW cm^{-2} and 1257 mW cm^{-2}, respectively, under 650 °C. Although promising, the exact role of such catalysts and the limitation of performance enhancement compared with that of H_2 fuel have not been studied in detail for high-performance direct ammonia fuel cells. Different fabrication techniques are also being considered to overcome the limitation posed by the lower ionic conductivity of proton-conducting fuel cell electrolytes. Pan et al.[108] synthesized a Ni-$BaZr_{0.1}Ce_{0.7}Y_{0.1}Yb_{0.1}$ (BZCYYb) anode by a phase-inversion method that is well known to form straight uniform pores throughout the material, thus facilitating gas transport. In conjunction with the BZCYYb electrolyte and $PrBa_{0.5}Sr_{0.5}Co_{1.5}Fe_{0.5}O_{5+\delta}$ (PBSCF) cathode, the cell produced an excellent power density of 1078 mW cm^{-2} at 700 °C. Thus, much effort is being invested in investigating different strategies for improving the power densities of DASOFCs. A summary of different cathodes, anodes, and electrolytes used for DASOFC and their performance has been provided in Table 1.

4 Approaches towards efficiency and long-term stability of DASOFCs

The long-term stability with better power densities and efficiency of DASOFCs is essential for scaling up the technology for industrial-scale applications. However, the efficiency of the DASOFC system is not high compared with SOFCs fueled with carbon-based fuels. To improve the stability and efficiency of the DASOFC system, high fuel utilization, fuel reforming technology, low overpotential cell materials, reduced system heat losses, and efficient BoP components to reduce excessive parasitic losses are crucial.[111] A detailed study on the improvement in DASOFC system efficiency was conducted by Selvam et al.[111] They have performed thermodynamic analyses and achieved a 12.17% higher energy efficiency of the SOFC system fueled with ammonia in full recirculation of a dead-end anode loop (71.95%) compared with the conventional configuration (59.78%). Kishimoto et al.[58] developed a 1 kW ammonia-fueled SOFC stack of 30 planar anode-supported cells. The stack fueled with direct

This journal is © the Partner Organisations 2023

Inorg. Chem. Front., 2023, 10, 6176–6192 | 6185

Table 1 Summary of best-performing cathodes, anodes, and electrolytes used for DASOFCs and their performance

Cathode	Anode	Electrolyte	Power density (W cm^{-2})	Temperature (°C)/ pressure (atm)	Ref.
$Pr_2B_2O_7$	NiO-YSZ	8YSZ	1.22	800/1	87
GDC-$La_{0.6}Sr_{0.4}CoO_3$	Ni-YSZ	8YSZ	0.83	750/1	82
			0.98	750/3	
ScSZ-LSM	Ni–Fe-YSZ|Ni-ScSZ	ScSZ	1.15	800/1	109
GDC-$NiCo_2O_4$	NiO-YSZ	8YSZ	1.06	800/1	78
$Mg_{0.4}NiMn_{1.6}O_4$	NiO-YSZ	8YSZ	0.20	600/1	110
LSC-GDC	NiO-YSZ	8YSZ	0.53	850/1	81
$Ba_{0.5}Sr_{0.5}Co_{0.8}Fe_{0.2}O_{3-\delta}$	Ni-SDC	SDC	1.19	650/1	33
$BaCo_{0.4}Fe_{0.4}Zr_{0.1}Y_{0.1}O_{3-\delta}$	$Pr_{0.6}Sr_{0.4}Co_{0.2}Fe_{0.75}Ru_{0.05}O_{3-\delta}$	SDC	0.50	800/1	86
$Sr_{1+x}Y_{2-x}O_{4+\delta}$-YSZ	NiO-YSZ	8YSZ	1.21	800/1	88
LSCF-GDC	Ni-GDC	8YSZ$_{PLD}$	1.33	650/1	62
Pt	NiO-$BaCe_{0.85}Eu_{0.15}O_3$	$BaCe_{0.8}Gd_{0.15}Pr_{0.05}O_{3-\delta}$	0.03	600/1	101
$Ba_{0.5}Sr_{0.5}Co_{0.8}Fe_{0.2}O_{3-\delta}$-$Ce_{0.8}Gd_{0.2}O_{1.9}$	Ni-$Ce_{0.8}Gd_{0.2}O_{1.9}$	$BaCe_{0.8}Gd_{0.2}O_{3-\delta}$	0.15	600/1	103
$Ba_{0.5}Sr_{0.5}Co_{0.8}Fe_{0.2}O_{3-\delta}$	NiO-$BaZr_{0.1}Ce_{0.7}Y_{0.2}O_{3-\delta}$	$BaZr_{0.1}Ce_{0.7}Y_{0.2}O_{3-\delta}$	0.39	750/1	104
LSCF	Pd	$BaZr_{0.1}Ce_{0.7}Y_{0.2}O_{3-\delta}$	0.58	600/1	105
$PrBa_{0.5}Sr_{0.5}Co_{1.5}Fe_{0.5}O_{5+\delta}$	Ni-$BaZr_{0.1}Ce_{0.7}Y_{0.1}Yb_{0.1}$	$BaZr_{0.1}Ce_{0.7}Y_{0.1}Yb_{0.1}$	0.11	700/1	108

ammonia achieved a 1 kW power output with 52% direct current (DC) electrical efficiency. A slight decrease in its performance compared with the stack with the hydrogen and nitrogen mixture fuel was attributed to the decline in the stack temperature caused by the endothermic ammonia decomposition reaction. As shown in Fig. 9(a), they have demonstrated the stable performance of the SOFC stack up to 1000 h by feeding direct ammonia. During stability studies, they observed a slight decrease in the average cell voltage at the beginning, but after 200 h, it became stable. The direct ammonia supply mode achieved a 690 W power output with 55.9% efficiency, indicating the feasibility of ammonia-fueled SOFC systems. Fig. 9(b) shows the photograph of the stack evaluation system fabricated by Noritake Co., Ltd (Japan) used for testing DASOFC performance, and Fig. 9(c) represents the 30 anode-supported cells with a diameter of 120 mm and an active area of 95 cm^2 of each cell.

They also performed a post-mortem analysis of the cells and separators by scanning electron microscope (SEM) and an electron probe micro analyzer. As shown in Fig. 10, the cross-section of the separator, including its surface on the anode side, is significantly deformed, and Fe-rich particles are observed on the surface. They also detected nitrogen in the SUS430 separator material, confirming that the separator was nitrided during the operation.

In another study, as shown in Fig. 11(a), Hagen et al.[112] assessed the stability for 1500 h of a single cell having the configuration Ni-YSZ/YSZ/LSM with the dimensions of 53 × 53 mm^2 and an active area of 16 cm^2 by fueling with pure ammonia at 850 °C. During the stability studies, they observed a reduced power output and electrical efficiency by 2–4%/1000 h. Okanishi et al.[113] demonstrated that the direct ammonia-fueled SOFC stack was stable for 1000 h at 777 °C without significant degradation. In their stack configuration, they have used a Ni/Y_2O_3-based catalyst for the ammonia decomposition and Co–Ce–Zr composite oxide catalyst for the autothermal ammonia cracking. They also observed an enhanced ammonia decomposition activity of Ni/Y_2O_3 by

Fig. 9 (a) Average cell voltage during a 1000 h durability test with ammonia fuel at 700 °C, 0.316 A cm^{-2} current density, the photograph of (b) the stack evaluation system and (c) the 30-cell SOFC stack. Reproduced with permission.[58] Copyright 2020, Wiley-VCH.
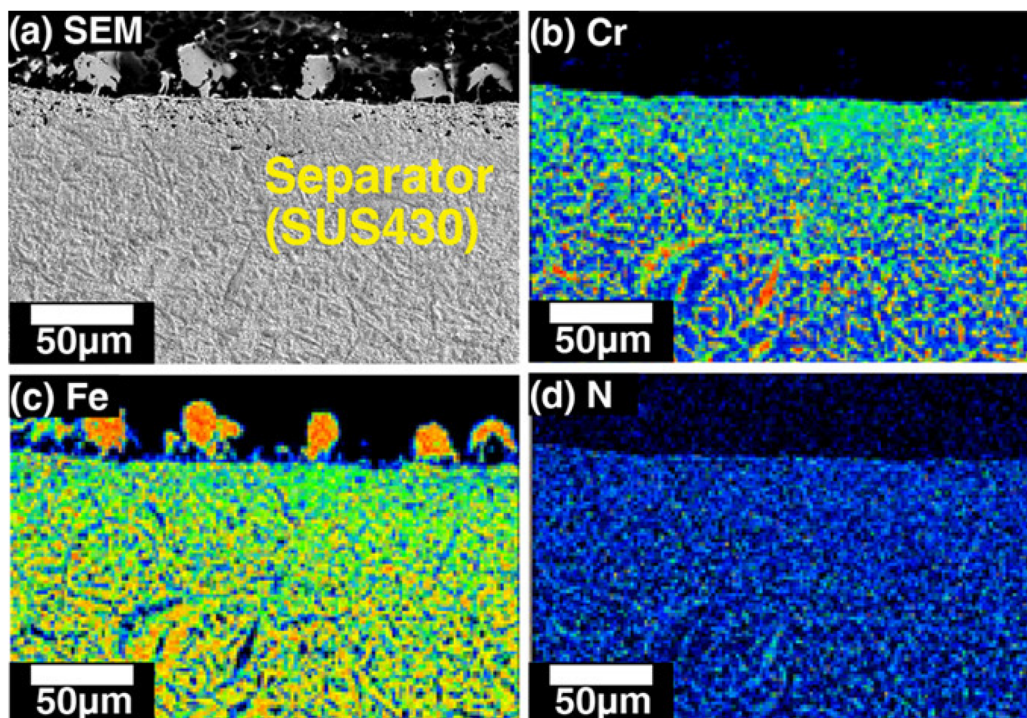
Fig. 10 Cross-sectional images of the separator on the anode side after a 1000 h durability test with direct ammonia fuel at 700 °C, 0.316 A cm^{-2} current density: (a) scanning electron microscopy image, and the distribution of (b) Cr, (c) Fe, and (d) N. Reproduced with permission.[58] Copyright 2020, Wiley-VCH.
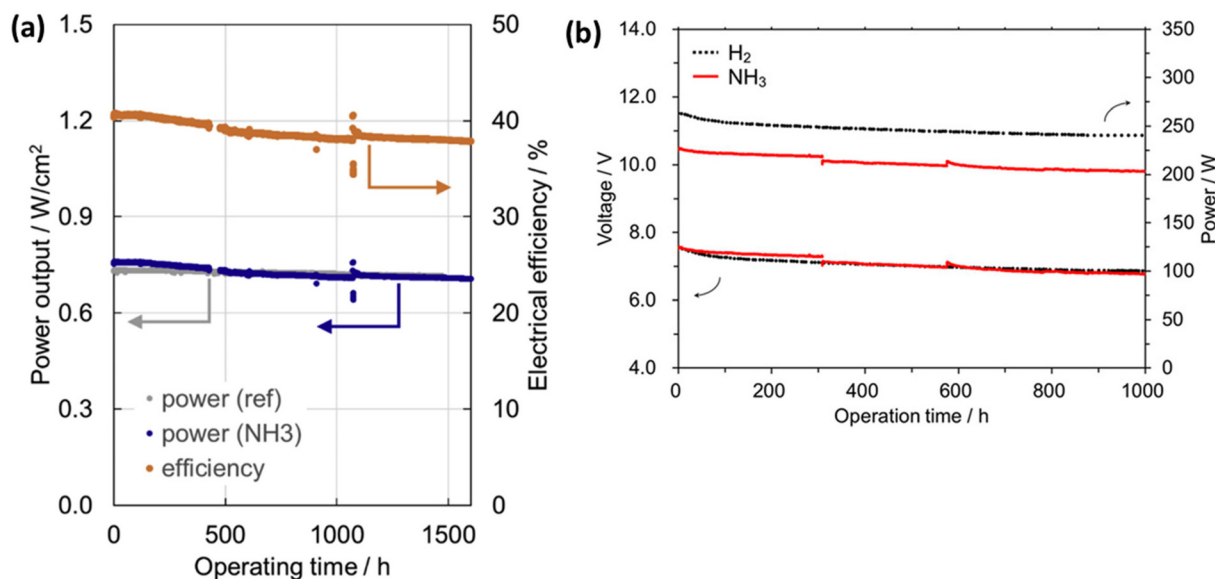

Fig. 11 (a) Power output (blue curve) and efficiency (orange curve) during the long-term test with ammonia fuel at 850 °C, 1 A cm^{-2} current density. Reproduced with permission.[112] Copyright 2019, Elsevier. (b) Time course of the voltage and power at 770 °C for the direct ammonia-fueled (red line) and H$_2$-fueled (black dotted line) SOFC stacks. The current was maintained at 30 and 35 A for the NH$_3$-fueled and the H$_2$-fueled ones, respectively. Reproduced with permission.[113] Copyright 2017, Wiley-VCH.

adding SrO. As shown in Fig. 11(b), the stability and power output of the direct ammonia-fueled stack is almost comparable to that of the H$_2$ fueled one. Additionally, the ammonia-fueled SOFC stack maintained more than 200 W power without significant degradation, demonstrating its feasibility on an industrial scale.

This journal is © the Partner Organisations 2023

Inorg. Chem. Front., 2023, **10**, 6176–6192 | **6187**

5 Challenges, opportunities, and future recommendations

5.1 Challenges

Renewable ammonia is a promising carbon-free fuel for SOFCs owing to the existence of an infrastructure and regulations for its production, transportation, and storage. SOFCs are receiving more interest for direct ammonia utilization as a fuel due to their high hydrogen content for power generation. Yet, because of the high-temperature operation, there are several technological challenges associated with DASOFCs, such as ammonia cracking, the possibility of NO_x formation at the anode, and coarsening of nickel and nitride formation in Ni-YSZ anode that can lead to microstructural changes and hampering of the anode activity and thus cell performance, which must be addressed through further research. More importantly, the anode must possess a sufficiently high porosity to allow the diffusion of fuel gas to the active sites and should also be conductive enough to allow the transfer of electrons. Another critical technological challenge in DASOFCs that must be addressed is the durability of the anode/electrolyte interface to achieve an extended period of operation. The other challenge is hydrogen dilution due to the presence of nitrogen (cracked ammonia) and steam formation in the anode chamber, which hinders the overall electrochemical performance. The sealing is another major issue, especially in the planar configuration, that needs to be rectified by finding suitable chemically and thermally compatible sealant materials.

5.2 Opportunities

Green ammonia as a hydrogen carrier has the potential to provide a substantial contribution to the goal of net zero emissions by 2050. Ammonia is currently the second most highly produced chemical globally. The projects about green ammonia synthesis are on a modest scale of tens of thousands of tons (4 GW plant by Air Products, ACWA Power, and NEOM, Saudi Arabia, to be operational by 2025,[114] and 1 GW by Yara Pilbara to be operational by 2030[115]), an order of magnitude smaller than a typical ammonia plant. The SOFC technology is quite mature (systems above 200 kW – *e.g.*, Bloom Energy) but needs to be tuned/optimized for ammonia fuel. The SOFC offers high electric and combined heat and power (CHP) efficiency with ammonia as a fuel for various distributed and centralized power applications. There is a widespread effort in developing technologies for the use of ammonia as an energy carrier and its potential use in SOFCs for power generation. Significant developments are underway today by IHI Corporation in Japan,[116] Haldor Topsoe in Denmark, Alma Norway,[117] and others.[118]

5.3 Future recommendations

Commercializing the DASOFC technology requires further investigations to overcome the technological challenges. For this purpose, developing novel electrodes and cell materials to convert ammonia directly into electric power efficiently is extremally important. Especially, ruthenium (Ru) is one of the highly active catalysts and could play a vital role in the future of ammonia decomposition/cracking at lower temperatures compared with a traditional Ni-based catalyst, leading to much lower energy consumption. Still, its expensive nature makes the large-scale development of Ru-based catalysts arduous. However, designing a new Ru-based catalyst by combining non-noble metals to exploit a synergic effect is possible. In addition, using proton-conducting electrolytes (H-SOFC) can mitigate the risk of NO_x emission and increase fuel utilization because of water vapor produced on the cathode side. Further investigations are required to confirm the impact of nickel nitriding on the cell and overall stack performance. Novel interconnects materials and barrier coating techniques must be developed to avoid cell material corrosion due to ammonia. Furthermore, developing novel sealing materials that can sustain exposure to ammonia at high temperatures, achieve high OCVs, and utilize ammonia is essential for developing this technology. Additionally, a careful design of cell configuration and operating conditions, including temperatures, is required to avoid cell material degradation. In addition, industrial-scale demonstrations are needed to leverage the potential of ammonia as a renewable energy carrier. Finally, the techno-economic model and bottom-up cost analysis of DASOFC systems need to be developed and provide technical and economic viability of electrode/electrolyte materials for commercializing DASOFCs.

6 Summary

In this review, we have covered the technological challenges associated with DASOFCs, recent advancements in state-of-the-art technology and newly emerging anode materials for DASOFCs, and future views/recommendations for the transition towards the future of ammonia as a source of power generation. Challenges and works in the synthesis and utilization of ammonia in the energy sector regarding use, safety, and economics are still under scrutiny at various levels. From a materials perspective, DASOFCs still rely on the ones being used in hydrogen-SOFCs, which include 8YSZ electrolytes, Ni-cermet anodes, and La-based perovskite cathodes. However, these traditional materials pose challenges like incomplete ammonia decomposition leading to a chain of undesired side reactions that not only cripples the cell performance but exacerbates its degradation alongside NO_x formation. Thus, research is being conducted in different directions to improve the power densities and stability of DASOFCs. This includes: (1) developing novel electrode/electrolyte materials (catalyst-infiltrated perovskites, pyrochlore oxides, fluorites, *etc.*) with higher ammonia decomposition activity, stability, and lesser NO_x forming propensity; (2) designing novel fabrication techniques (like pulsed laser deposition, phase inversion techniques, and atomic layer deposition) to achieve highly controlled nanostructured electrode surfaces with straight uniform pores that not only improve the electrode–electrolyte

6188 | *Inorg. Chem. Front.*, 2023, **10**, 6176–6192

This journal is © the Partner Organisations 2023

interfacial microstructure but also improve gas adsorption/desorption and gas diffusion, thus enhancing the overall cell kinetics; and (3) optimizing the operating conditions like temperature and pressure to maximize power densities and stability. The highest power density reported is reasonably high (1190 mW cm^{-2} at 800 °C using a 10 μm thick SDC electrolyte, BSCF cathode, and Ni-SDC anode), but these need to be demonstrated on a larger scale of cells/stacks with stable performance. As a final remark, it is clear that ammonia will play a significant role in the future energy mix due to its favorable physical properties and the existing infrastructure for its transport, storage, and distribution. However, many safety and technological challenges exist before ammonia is commercially deployed as a primary energy vector. The combination of green ammonia production and its utilization will form the critical parts of the ammonia economy.

Abbreviations

BECCS	Bioenergy combined with carbon capture and storage
CHP	Combined heat and power
CCS	Carbon capture and storage
CO_2	Carbon dioxide
DASOFCs	Direct ammonia solid oxide fuel cells
Gt	Gigatonne
GDC	Gadolinium-doped ceria
H_2O	Water
H_2	Hydrogen
H–B	Haber–Bosch
H-DASOFC	Proton-conducting electrolyte-based direct ammonia solid oxide fuel cell
H-SOFC	Proton-conducting solid-oxide fuel cell
IRENA	International Renewable Energy Agency
kW	Kilowatt
LSCF	Lanthanum strontium cobalt ferrite
SEM	Scanning electron microscopy
SOFCs	Solid oxide fuel cells
TW	Terawatt
OCV	Open circuit voltage
O-SOFC	Oxygen ion-conducting solid-oxide fuel cell
O-DASOFC	Oxide-ion-conducting electrolyte-based direct ammonia solid oxide fuel cell
N_2	Nitrogen
NH_3	Ammonia
Ni-YSZ	Nickel oxide–yttria-stabilized zirconia
Ni_3N	Nickel nitride
NO_x	Nitrous oxide
XRD	X-ray diffraction
YSZ	Yttria-stabilized zirconia

Conflicts of interest

There are no conflicts to declare.

Acknowledgements

References

1 https://ourworldindata.org/co2-emissions.
2 S. Lewis Nathan and G. Nocera Daniel, *Proc. Natl. Acad. Sci. U. S. A.*, 2006, **103**, 15729–15735.
3 M. S. Dresselhaus and I. L. Thomas, *Nature*, 2001, **414**, 332–337.
4 https://www.un.org/en/climatechange/paris-agreement.
5 https://www.irena.org/publications/2022/Mar/World-Energy-Transitions-Outlook-2022.
6 R. R. Ratnakar, N. Gupta, K. Zhang, C. van Doorne, J. Fesmire, B. Dindoruk and V. Balakotaiah, *Int. J. Hydrogen Energy*, 2021, **46**, 24149–24168.
7 Y. Zhao, B. P. Setzler, J. Wang, J. Nash, T. Wang, B. Xu and Y. Yan, *Joule*, 2019, **3**, 2472–2484.
8 S. Sorcar, H. Zinowits, E. P. Komarala, N. Moshe, I. Agranovich and B. A. Rosen, *J. Mater. Chem. A*, 2022, **10**, 24115–24126.
9 https://www.thechemicalengineer.com/features/h2-and-nh3-the-perfect-marriage-in-a-carbon-free-society/.
10 D. R. MacFarlane, P. V. Cherepanov, J. Choi, B. H. R. Suryanto, R. Y. Hodgetts, J. M. Bakker, F. M. Ferrero Vallana and A. N. Simonov, *Joule*, 2020, **4**, 1186–1205.
11 A. Valera-Medina, H. Xiao, M. Owen-Jones, W. I. F. David and P. J. Bowen, *Prog. Energy Combust. Sci.*, 2018, **69**, 63–102.
12 G. G. M. Fournier, I. W. Cumming and K. Hellgardt, *J. Power Sources*, 2006, **162**, 198–206.
13 S. Giddey, S. P. S. Badwal, C. Munnings and M. Dolan, *ACS Sustainable Chem. Eng.*, 2017, **5**, 10231–10239.
14 Y. Kojima, *Int. J. Hydrogen Energy*, 2019, **44**, 18179–18192.
15 Eneus Energy, The green ammonia landscape, website accessed July 2023. https://www.eneusenergy.com/why-ammonia/.
16 Technology|The Green Ammonia Landscape, https://www.eneusenergy.com/technology/.
17 R. M. Nayak-Luke, Z. Cesaro and R. Bañares-Alcántara, in *Techno-Economic Challenges of Green Ammonia as an Energy Vector*, ed. A. Valera-Medina and R. Banares-Alcantara, Academic Press, 2021, pp. 27–39, DOI: 10.1016/B978-0-12-820560-0.00003-5.
18 https://newatlas.com/energy/green-ammonia-phosphonium-production/.
19 H. Ju, D. H. Seo, S. Chung, X. Mao, B.-S. An, M. Musameh, T. R. Gengenbach, H. Shon, A. Du, A. Bendavid, K. Ostrikov, H. C. Yoon, J. Lee and S. Giddey, *Nanoscale*, 2022, **14**, 1395–1408.

This journal is © the Partner Organisations 2023

Inorg. Chem. Front., 2023, **10**, 6176–6192 | **6189**

20 B. H. R. Suryanto, K. Matuszek, J. Choi, R. Y. Hodgetts, H.-L. Du, J. M. Bakker, C. S. M. Kang, P. V. Cherepanov, A. N. Simonov and D. R. MacFarlane, *Science*, 2021, **372**, 1187–1191.

21 A. J. Reiter and S.-C. Kong, *Fuel*, 2011, **90**, 87–97.

22 V. Alagharu, S. Palanki and K. N. West, *J. Power Sources*, 2010, **195**, 829–833.

23 S. S. Rathore, A. P. Kulkarni, D. Fini, S. Giddey and A. Seeber, *Solids*, 2021, **2**, 177–191.

24 J. Yang, A. F. S. Molouk, T. Okanishi, H. Muroyama, T. Matsui and K. Eguchi, *ACS Appl. Mater. Interfaces*, 2015, **7**, 7406–7412.

25 S. S. Rathore, S. Biswas, D. Fini, A. P. Kulkarni and S. Giddey, *Int. J. Hydrogen Energy*, 2021, **46**, 35365–35384.

26 E. J. Cairns, E. L. Simons and A. D. Tevebaugh, *Nature*, 1968, **217**, 780–781.

27 C. G. Vayenas and R. D. Farr, *Science*, 1980, **208**, 593–594.

28 K. H. M. Al-Hamed and I. Dincer, *Energy*, 2021, **220**, 119771.

29 K. Miyazaki, T. Okanishi, H. Muroyama, T. Matsui and K. Eguchi, *J. Power Sources*, 2017, **365**, 148–154.

30 G. Jeerh, P. Zou, M. Zhang and S. Tao, *Appl. Catal., B*, 2022, **319**, 121919.

31 S. S. Katikaneni, K. Lee, L. Kangyong, J. Bae and W. C. Jung, Direct ammonia-fed solid oxide fuel cell and methods for making the same, *US Patent App* 17/367871, 2022.

32 G. Cinti, G. Discepoli, E. Sisani and U. Desideri, *Int. J. Hydrogen Energy*, 2016, **41**, 13583–13590.

33 G. Meng, C. Jiang, J. Ma, Q. Ma and X. Liu, *J. Power Sources*, 2007, **173**, 189–193.

34 Y. Luo, S. Liao, S. Chen, H. Fang, F. Zhong, L. Lin, C. Zhou, C. Chen, G. Cai, C.-T. Au and L. Jiang, *Appl. Energy*, 2022, **307**, 118158.

35 M. Zendrini, M. Testi, M. Trini, P. Daniele, J. Van Herle and L. Crema, *Int. J. Hydrogen Energy*, 2021, **46**, 30112–30123.

36 J. Yang, A. F. S. Molouk, T. Okanishi, H. Muroyama, T. Matsui and K. Eguchi, *ACS Appl. Mater. Interfaces*, 2015, **7**, 28701–28707.

37 C. T. Sigal and C. G. Vayenas, *Solid State Ionics*, 1981, **5**, 567–570.

38 R. Lan and S. Tao, *Front. Energy Res.*, 2014, **2**, 1–4.

39 A. Afif, N. Radenahmad, Q. Cheok, S. Shams, J. H. Kim and A. K. Azad, *Renewable Sustainable Energy Rev.*, 2016, **60**, 822–835.

40 G. Jeerh, M. Zhang and S. Tao, *J. Mater. Chem. A*, 2021, **9**, 727–752.

41 M. Asmare, M. Ilbas and S. Yalcin, *Int. J. Hydrogen Energy*, 2021, **46**, 36878–36889.

42 M. Sonker, S. K. Tiwary, N. Shreyash, S. Bajpai, M. Ray, S. K. Kar and M. S. Balathanigaimani, *J. Cleaner Prod.*, 2022, **376**, 133960.

43 A. Valera-Medina, F. Amer-Hatem, A. K. Azad, I. C. Dedoussi, M. de Joannon, R. X. Fernandes, P. Glarborg, H. Hashemi, X. He, S. Mashruk, J. McGowan, C. Mounaim-Rouselle, A. Ortiz-Prado, A. Ortiz-Valera, I. Rossetti, B. Shu, M. Yehia, H. Xiao and M. Costa, *Energy Fuels*, 2021, **35**, 6964–7029.

44 S. Oh, M. J. Oh, J. Hong, K. J. Yoon, H.-I. Ji, J.-H. Lee, H. Kang, J.-W. Son and S. Yang, *iScience*, 2022, **25**, 105009.

45 Z. Wan, Y. Tao, J. Shao, Y. Zhang and H. You, *Energy Convers. Manage.*, 2021, **228**, 113729.

46 M. Fecke, S. Garner and B. Cox, *Review of global regulations for anhydrous ammonia production, use, and storage*, Hazards 26, IChemE, Rugby, 2016, https://www.icheme.org/media/11771/hazards-26-paper-34-review-ofglobal-regulations-for-anhydrous-ammonia-production-use-and-storage.pdf.

47 https://www.cdc.gov/niosh/idlh/intridl4.html.

48 A. Klerke, C. H. Christensen, J. K. Nørskov and T. Vegge, *J. Mater. Chem.*, 2008, **18**, 2304–2310.

49 W. Akimoto, M. Saito, M. Inaba, H. Yoshida and T. Inagaki, *ECS Trans.*, 2013, **57**, 1639.

50 A. Fuerte, R. X. Valenzuela, M. J. Escudero and L. Daza, *J. Power Sources*, 2009, **192**, 170–174.

51 I. Lucentini, X. Garcia, X. Vendrell and J. Llorca, *Ind. Eng. Chem. Res.*, 2021, **60**, 18560–18611.

52 M. Nagamori, T. Shimonosono, S. Sameshima, Y. Hirata, N. Matsunaga and Y. Sakka, *J. Am. Ceram. Soc.*, 2009, **92**, S117–S121.

53 Y. Zhang and C. Xia, *J. Power Sources*, 2010, **195**, 6611–6618.

54 F. Tietz, *Ionics*, 1999, **5**, 129–139.

55 M. Tatko, M. Mosiałek, A. Kędra, E. Bielańska, M. Ruggiero-Mikołajczyk and P. Nowak, *J. Solid State Electrochem.*, 2016, **20**, 143–151.

56 B. Stoeckl, V. Subotić, M. Preininger, M. Schwaiger, N. Evic, H. Schroettner and C. Hochenauer, *Electrochim. Acta*, 2019, **298**, 874–883.

57 Y. Kalinci and I. Dincer, *Int. J. Hydrogen Energy*, 2018, **43**, 5795–5807.

58 M. Kishimoto, H. Muroyama, S. Suzuki, M. Saito, T. Koide, Y. Takahashi, T. Horiuchi, H. Yamasaki, S. Matsumoto, H. Kubo, N. Takahashi, A. Okabe, S. Ueguchi, M. Jun, A. Tateno, T. Matsuo, T. Matsui, H. Iwai, H. Yoshida and K. Eguchi, *Fuel Cells*, 2020, **20**, 80–88.

59 K. Miyazaki, H. Muroyama, T. Matsui and K. Eguchi, *Sustainable Energy Fuels*, 2020, **4**, 5238–5246.

60 H. Kobayashi, A. Hayakawa, K. D. Kunkuma, A. Somarathne and E. C. Okafor, *Proc. Combust. Inst.*, 2019, **37**, 109–133.

61 J. Yang, T. Akagi, T. Okanishi, H. Muroyama, T. Matsui and K. Eguchi, *Fuel Cells*, 2015, **15**, 390–397.

62 S. Oh, M. J. Oh, J. Hong, K. J. Yoon, H.-I. Ji, J.-H. Lee, H. Kang, J.-W. Son and S. Yang, *Science*, 2022, **25**, 105009.

63 D.-H. Myung, J. Hwang, J. Hong, H.-W. Lee, B.-K. Kim, J.-H. Lee and J.-W. Son, *J. Electrochem. Soc.*, 2011, **158**, B1000.

64 C.-C. Chao, C.-M. Hsu, Y. Cui and F. B. Prinz, *ACS Nano*, 2011, **5**, 5692–5696.

6190 | *Inorg. Chem. Front.*, 2023, **10**, 6176–6192

This journal is © the Partner Organisations 2023

65 A. Karimaghaloo, J. Koo, H.-S. Kang, S. Song, J. H. Shim and M. H. Lee, *Int. J. Precis. Eng. Manuf. - Green Technol.*, 2019, **6**, 611–628.

66 P.-C. Su, C.-C. Chao, J. H. Shim, R. Fasching and F. B. Prinz, *Nano Lett.*, 2008, **8**, 2289–2292.

67 J. H. Shim, C.-C. Chao, H. Huang and F. B. Prinz, *Chem. Mater.*, 2007, **19**, 3850–3854.

68 J. H. Shim, G. D. Han, H. J. Choi, Y. Kim, S. Xu, J. An, Y. B. Kim, T. Graf, T. D. Schladt and T. M. Gür, *Int. J. Precis. Eng. Manuf. - Green Technol.*, 2019, **6**, 629–646.

69 J. An, Y.-B. Kim, J. Park, T. M. Gür and F. B. Prinz, *Nano Lett.*, 2013, **13**, 4551–4555.

70 K. S. Weil, *JOM*, 2006, **58**, 37–44.

71 C. Vayenas and R. Farr, *Science*, 1980, **208**, 593–594.

72 A. Wojcik, H. Middleton, I. Damopoulos and J. Van herle, *J. Power Sources*, 2003, **118**, 342–348.

73 Y. Song, H. Li, M. Xu, G. Yang, W. Wang, R. Ran, W. Zhou and Z. Shao, *Small*, 2020, **16**, 2001859.

74 Q. Ma, R. Peng, L. Tian and G. Meng, *Electrochem. Commun.*, 2006, **8**, 1791–1795.

75 M. Hashinokuchi, R. Yokochi, W. Akimoto, T. Doi, M. Inaba and J. Kugai, *ECS Trans.*, 2015, **68**, 2739.

76 W. Akimoto, T. Fujimoto, M. Saito, M. Inaba, H. Yoshida and T. Inagaki, *Solid State Ionics*, 2014, **256**, 1–4.

77 H. Kildahl, H. Cao and Y. Ding, *Energy Storage Sav.*, 2022, **1**, 309–324.

78 F. Zhong, Z. Li, Y. Luo, H. Fang, K. Chen, C. Zhou, C. Chen, L. Lin and L. Jiang, *Int. J. Green Energy*, 2022, 1–10, DOI: **10.1080/15435075.2021.2018324**.

79 Q. Xu, Z. Guo, L. Xia, Q. He, Z. Li, I. T. Bello, K. Zheng and M. Ni, *Energy Convers. Manage.*, 2022, **253**, 115175.

80 K. Okura, T. Okanishi, H. Muroyama, T. Matsui and K. Eguchi, *ChemCatChem*, 2016, **8**, 2988–2995.

81 Q. Ma, J. Ma, S. Zhou, R. Yan, J. Gao and G. Meng, *J. Power Sources*, 2007, **164**, 86–89.

82 S. Shy, S. Hsieh and H. Chang, *J. Power Sources*, 2018, **396**, 80–87.

83 P. C. Wu and S. S. Shy, *J. Power Sources*, 2017, **362**, 105–114.

84 S. S. Rathore, A. P. Kulkarni, D. Fini, S. Giddey and A. Seeber, *Journal*, 2021, **2**, 177–191.

85 J. Cavazzani, E. Squizzato, E. Brusamarello and A. Glisenti, *Int. J. Hydrogen Energy*, 2022, **47**, 13921–13932.

86 X. Xiong, J. Yu, X. Huang, D. Zou, Y. Song, M. Xu, R. Ran, W. Wang, W. Zhou and Z. Shao, *J. Mater. Sci. Technol.*, 2022, **125**, 51–58.

87 F. Zhong, S. Yang, C. Chen, H. Fang, K. Chen, C. Zhou, L. Lin, Y. Luo, C. Au and L. Jiang, *J. Power Sources*, 2022, **520**, 230847.

88 F. Zhong, Y. Zhang, Y. Luo, C. Chen, H. Fang, K. Chen, C. Zhou, L. Lin, C. Au and L. Jiang, *J. Power Sources*, 2022, **524**, 231078.

89 S.-C. Jung, K.-H. Chung, J. Choi, Y.-K. Park, S.-J. Kim, B.-J. Kim and H. Lee, *Catal. Today*, 2022, **397**, 165–172.

90 C. Chen, K. Wu, H. Ren, C. Zhou, Y. Luo, L. Lin, C. Au and L. Jiang, *Energy Fuels*, 2021, **35**, 11693–11706.

91 S. Peters, A. M. Abdel-Mageed and S. Wohlrab, *ChemCatChem*, 2023, **15**, e202201185.

92 M. Abashar, Y. Al-Sughair and I. Al-Mutaz, *Appl. Catal., A*, 2002, **236**, 35–53.

93 G. b. Lente, *ACS Catal.*, 2013, **3**, 381–382.

94 S. Biswas, C. Kundu, W. L. Ng, S. P. Samudrala, T. Jarvis, S. Giddey and S. Bhattacharya, *J. CO₂ Util.*, 2023, **72**, 102501.

95 M. Ni, M. K. Leung and D. Y. Leung, *Int. J. Energy Res.*, 2009, **33**, 943–959.

96 K. Miyazaki, T. Okanishi, H. Muroyama, T. Matsui and K. Eguchi, *J. Power Sources*, 2017, **365**, 148–154.

97 D. Medvedev, J. Lyagaeva, E. Gorbova, A. Demin and P. Tsiakaras, *Prog. Mater. Sci.*, 2016, **75**, 38–79.

98 J. Fish, S. Ricote, R. O'Hayre and N. Bonanos, *J. Mater. Chem. A*, 2015, **3**, 5392–5401.

99 C.-J. Tseng, J.-K. Chang, K.-R. Lee, I.-M. Hung, J.-C. Lin, S.-C. Jang and S.-W. Lee, *J. Alloys Compd.*, 2017, **696**, 251–256.

100 K.-R. Lee, C.-J. Tseng, J.-K. Chang, I.-M. Hung, J.-C. Lin and S.-W. Lee, *Int. J. Hydrogen Energy*, 2013, **38**, 11097–11103.

101 N. Maffei, L. Pelletier and A. McFarlan, *J. Power Sources*, 2008, **175**, 221–225.

102 L. Pelletier, A. McFarlan and N. Maffei, *J. Power Sources*, 2005, **145**, 262–265.

103 L. Zhang and W. Yang, *J. Power Sources*, 2008, **179**, 92–95.

104 Y. Lin, R. Ran, Y. Guo, W. Zhou, R. Cai, J. Wang and Z. Shao, *Int. J. Hydrogen Energy*, 2010, **35**, 2637–2642.

105 Y. Aoki, T. Yamaguchi, S. Kobayashi, D. Kowalski, C. Zhu and H. Habazaki, *Global Challenges*, 2018, **2**, 1700088.

106 F. He, Q. Gao, Z. Liu, M. Yang, R. Ran, G. Yang, W. Wang, W. Zhou and Z. Shao, *Adv. Energy Mater.*, 2021, **11**, 2003916.

107 H. Zhang, Y. Zhou, K. Pei, Y. Pan, K. Xu, Y. Ding, B. Zhao, K. Sasaki, Y. Choi and Y. Chen, *Energy Environ. Sci.*, 2022, **15**, 287–295.

108 Y. Pan, H. Zhang, K. Xu, Y. Zhou, B. Zhao, W. Yuan, K. Sasaki, Y. Choi, Y. Chen and M. Liu, *Appl. Catal., B*, 2022, **306**, 121071.

109 L. Liu, K. Sun, X. Wu, X. Li, M. Zhang, N. Zhang and X. Zhou, *Int. J. Hydrogen Energy*, 2012, **37**, 10857–10865.

110 F. Zhong, C. Han, Y. Luo, C. Zhou, C. Chen, L. Lin, G. Cai and L. Jiang, *J. Power Sources*, 2021, **503**, 230020.

111 K. Selvam, Y. Komatsu, A. Sciazko, S. Kaneko and N. Shikazono, *Energy Convers. Manage.*, 2021, **249**, 114839.

112 A. Hagen, H. Langnickel and X. Sun, *Int. J. Hydrogen Energy*, 2019, **44**, 18382–18392.

113 T. Okanishi, K. Okura, A. Srifa, H. Muroyama, T. Matsui, M. Kishimoto, M. Saito, H. Iwai, H. Yoshida, M. Saito, T. Koide, H. Iwai, S. Suzuki, Y. Takahashi, T. Horiuchi, H. Yamasaki, S. Matsumoto, S. Yumoto, H. Kubo, J. Kawahara, A. Okabe, Y. Kikkawa, T. Isomura and K. Eguchi, *Fuel Cells*, 2017, **17**, 383–390.

114 Saudi Arabia to export renewable energy using green ammonia, **https://www.ammoniaenergy.org/articles/saudi-arabia-to-export-renewable-energy-using-green-ammonia/**.

This journal is © the Partner Organisations 2023

Inorg. Chem. Front., 2023, **10**, 6176–6192 | **6191**

115 Green ammonia plants win financing in Australia and New Zealand, https://www.ammoniaenergy.org/articles/green-ammonia-plants-win-financing-in-australia-and-new-zealand/#:~:text=In%20recent%20weeks%2C%20governments%20in,ammonia%20pilot%20at%20Yara%20Pilbara.

116 IHI Corporation, 2018 Demonstration of World-Leading Ammonia Mixed Combustion at Combustion Test Facility for Coal-Fired Power Plant-Development of Combustion Technology Enabling Use of Ammonia as Fuel, Contributing to Reduction of CO$_2$ Emissions, see https://www.ihi.co.jp/ihi/all_news/2017/technology/2018-3-28/index.html.

117 https://www.offshore-energy.biz/alma-clean-power-tests-6-kw-direct-ammonia-fuel-cell-system/.

118 https://dev.ammoniaenergy.org/organization/ihi-corporation/.

6192 | *Inorg. Chem. Front.*, 2023, **10**, 6176–6192

This journal is © the Partner Organisations 2023